

Article

Corrosion Behavior of Passivated Martensitic and Semi-Austenitic Precipitation Hardening Stainless Steel

Facundo Almeraya-Calderón ^{1,*}, Oliver Samaniego-Gómez ¹, Erick Maldonado-Bandala ², Demetrio Nieves-Mendoza ², Javier Olguín-Coca ³, Jesús Manuel Jáquez-Muñoz ¹, José Cabral-Miramontes ¹, Juan Pablo Flores-De los Ríos ⁴, Raul German Bautista-Margulis ^{5,*} and Citlalli Gaona-Tiburcio ¹

- ¹ FIME-Centro de Investigación e Innovación en Ingeniería Aeronáutica (CIIA), Universidad Autónoma de Nuevo León, Av. Universidad s/n, Ciudad Universitaria, San Nicolás de los Garza 66455, Mexico; pedro.samaniegom@uanl.edu.mx (O.S.-G.); jesus.jaquezmn@uanl.edu.mx (J.M.J.-M.); jose.cabralmr@uanl.edu.mx (J.C.-M.); citlalli.gaonatbr@uanl.edu.mx (C.G.-T.)
- ² Facultad de Ingeniería Civil, Universidad Veracruzana, Xalapa 91000, Mexico; erimaldonado@uv.mx (E.M.-B.); dnieves@uv.mx (D.N.-M.)
- ³ Área Académica de Ingeniería y Arquitectura, Universidad Autónoma del Estado de Hidalgo, 42082 Carretera Pachuca-Tulancingo Km. 4.5., Pachuca de Soto 42082, Mexico; olguinc@uaeh.edu.mx
- ⁴ Department Metal-Mechanical, Tecnológico Nacional de México-Instituto Tecnológico de Chihuahua, Av. Tecnológico 2909, Chihuahua 31130, Mexico; juan.fd@chihuahua.tecnm.mx
- ⁵ División Académica de Ciencias Biológicas, Universidad Juárez Autónoma de Tabasco, Villahermosa 86040, Mexico
- * Correspondence: facundo.almerayacl@uanl.edu.mx (F.A.-C.); margulisrg@hotmail.com (R.G.B.-M.)



Citation: Almeraya-Calderón, F.; Samaniego-Gómez, O.; Maldonado-Bandala, E.; Nieves-Mendoza, D.; Olguín-Coca, J.; Jáquez-Muñoz, J.M.; Cabral-Miramontes, J.; Flores-De los Ríos, J.P.; Bautista-Margulis, R.G.; Gaona-Tiburcio, C. Corrosion Behavior of Passivated Martensitic and Semi-Austenitic Precipitation Hardening Stainless Steel. *Metals* **2022**, *12*, 1033. <https://doi.org/10.3390/met12061033>

Academic Editors: Antonio Collazo and Alexandre Emelyanenko

Received: 12 May 2022

Accepted: 11 June 2022

Published: 17 June 2022

Publisher's Note: MDPI stays neutral with regard to jurisdictional claims in published maps and institutional affiliations.



Copyright: © 2022 by the authors. Licensee MDPI, Basel, Switzerland. This article is an open access article distributed under the terms and conditions of the Creative Commons Attribution (CC BY) license (<https://creativecommons.org/licenses/by/4.0/>).

Abstract: This research aimed to conduct a passive layer state study on martensitic and semi-austenitic precipitation hardening stainless steels (PHSS) passivated in citric acid and nitric acid baths at 49 and 70 °C for 50 and 75 min and subsequently exposed in 5 wt.% NaCl and 1 wt.% H₂SO₄ solutions. Corrosion behavior of the passivated material was observed by using potentiodynamic polarization (PP) according to the ASTM G5-11 standard. The microstructural analysis was performed by optical microscopy and scanning electron microscopy (SEM), while the passivated layer was characterized by X-ray photoelectron spectroscopy (XPS). The results indicated that the semi-austenitic-NA-50 min-70 °C sample showed the best corrosion resistance behavior in both solutions. The XPS characterization confirmed that the martensitic and semi-austenitic surface film presented a mixture of chemical compounds, such as Cr₂O₃ and Fe(OH)O, respectively.

Keywords: martensitic and semi-austenitic; PH stainless steel; passivation; potentiodynamic polarization; X-ray photoelectron spectroscopy

1. Introduction

Corrosion deterioration of materials in the aircraft industry is a major problem affecting economic, safety, and logistical issues. Corrosion protection methods seek to be friendly to the environment due to the demands in the aeronautical sector. Passivation treatment is a protection method commonly used in stainless steels (SS) to increase their corrosion resistance [1–4]. Stainless steels are widely used in the industry due to their excellent mechanical resistance, corrosion resistance, and impact resistance.

According to their microstructures, stainless steels are classified into ferritic (α), martensitic (α'), austenitic (γ), duplex (mixture of ferrite and austenite), and precipitation hardening (PH) [1,5,6]. Three main types are typically used in the aeronautical industry: austenitic, martensitic, and PH stainless steel. Good performance in aggressive environments has been observed due to their corrosion, mechanical, and high-temperature properties. They can be used in aircraft components such as actuators, fasteners, and landing gear supports [6–8]. Aeronautical materials such as stainless steel are used in

various components and are commonly exposed to different atmospheres such as industrial and marine.

The precipitation hardening stainless steels (PHSS) are a group with excellent corrosion-resistant alloys that can be heat-treated with precipitation hardening, also called aging, to provide high tensile strength. The alloying elements of these steels are Chromium, the main element to form the protective passivation layer, and Nickel, which helps stabilize the austenitic phase and improve mechanical resistance. Furthermore, in small amounts of other metals, additional elements include Molybdenum, which helps to improve localized corrosion resistance, and Tungsten, Aluminum, Titanium, and Niobium can form intermetallic compounds to improve mechanical resistance [1,9,10]. According to the parent phase, PH stainless steels are grouped into three main classes austenitic (γ), semi-austenitic (γ and δ), and martensitic (α'). The chemical composition is the main reason for obtaining excellent properties and the final microstructure of the PHSS [11–16].

The semi-austenitic grades PHSS basically austenitic with annealed treatment. Austenitic PHSS features an austenitic phase in both the age-treated and annealed conditions. Martensitic PHSS is also called single-treatment steel and has a martensitic microstructure. After aging treatment, the martensitic and semi-austenitic PHSS can reach tensile strengths greater than 1300 MPa. However, they decrease ductility when passing from the annealed to the aged-treated condition. For values around 950 MPa, however, austenitic PHSS does not have ductility by high mechanical strength after aging treatment. In the aerospace sector, martensitic and austenitic stainless steels are limited to specific components due to the tribological properties of these steels. Stainless steels 17-4PH, 17-7PH and 15-7Mo were introduced by Armco (Middletown, OH, USA) in 1948. Nevertheless, years later, PHSS steels such as AM350 and AM355 (both semi-austenitic), Custom 630, Custom 455, and Custom450 (all martensitic) were developed [17,18].

The alloying element that provides corrosion resistance in stainless steel is chromium, which reacts with oxygen and forms a protective surface layer based on chromium oxide (Cr_2O_3) [19,20]. Passivation is a chemical process used on stainless steel with an oxidant agent, according to specification ASTM A967 [21]. However, an alternative to nitric acid passivation is citric acid because it is non-toxic and biodegradable. Based on the literature, it is observed that there is scarce information on the benefits of using citric acid in the passivation of stainless steels [22–25]. The Boeing Company evaluated the use of citric acid as an alternative for the passivation of stainless steel in aeronautical components [26]. In 2008, the National Aeronautics and Space Administration (NASA) began a research project evaluating the use of nitric acid in the passivation treatment of welded parts, using accelerated tests such as a salt chamber [27]. Likewise, the effectiveness of using citric acid to passivate stainless steel has also been reported [28].

A number of investigations of stainless steels have been focused on their corrosion behavior, such as passivation, corrosion rates, pitting nucleation potentials, transpassive regions, and corrosion mechanisms. Typical electrochemical techniques of DC and AC are galvanodynamic (PG), potentiodynamic (PP), cyclic potentiodynamic polarization (PPC), electrochemical impedance spectroscopy (EIS), and electrochemical noise (EN).

The AISI 304 SS corrosion in ferric chloride (FeCl_3) solution using electrochemical noise was studied by Suresh and Mudali [29]. The results indicated a relationship between the frequency domain (power spectral density, PSD) and time-domain (statistical analysis) that determines the localized corrosion mechanism. Lara et al. [30] evaluated the passivated 15-5PH and 17-4PH SS employing EN and PPC. The results indicated that a similar passive layer formed in both passivating acid solutions. Bragaglia et al. [31] used PP to determine the behavior of passivated and unpassivated 304 SS austenitic in acid solutions. The pitting potential increased with the passivation, particularly nitric acid.

Marcelin et al. [32] studied the characterization of the electrochemical behavior of martensitic stainless steel; the results indicated that the corrosion process was controlled by passive film properties formed during air exposure. Impedance diagrams allowed the characterization of the oxide film and the charge transfer process.

In 2004, El-Taib Heakal et al. [33] concluded that the effect of pH on the electrochemical behavior of austenitic stainless steels in naturally aerated and nitrogen-deaerated buffer solutions was studied. Potentiodynamic polarization and electrochemical impedance spectroscopy techniques were used. The results indicate that corrosion current (i_{corr}) decreases with pH due to an effect of alloying elements such as molybdenum. Ameer et al. [34] reported potentiodynamic polarization results showed that i_{corr} and i_c increase with increasing either Cl^- or SO_4^{2-} concentration, indicating the decrease in the passivity of the formed film. The stability of naturally grown passive films on Mo-containing stainless steel was studied by El-Taib Heakal et al. [35] in aerated and deaerated buffer solutions with different pH and in sulfate and chloride solutions. Analysis of the EIS data indicates that the total resistance (RT) of the passive film has higher values in aerated solutions and is generally lower in basic solutions. This indicates that lower solution pH favors the formation of oxide films, offering better corrosion resistance. The higher values of RT in Na_2SO_4 solutions suggest the formation of more stable passive films in sulfate than in chloride solutions.

Recent investigations on PHSS have focused on hydrogen diffusion, fatigue behavior, and microstructural characterization [36–45]. Samaniego et al. [46] studied the corrosion behavior of CUSTOM450 and AM350 passivated PHSS steels using electrochemical noise and electrochemical impedance spectroscopy in acid baths. The CUSTOM 450 PHSS showed the best results for corrosion behavior in acid baths.

This work aimed to study the passive state of martensitic and semi-austenitic PHSS passivated in citric and nitric acid baths at 49 and 70 °C for 50 and 75 min, immersed in 5 wt.% NaCl and 1 wt.% H_2SO_4 solutions, applying potentiodynamic polarization (PP). The microstructural analysis was performed by scanning electron microscopy (SEM) and optical microscopy (OM). The passivated layer was characterized by X-ray photoelectron spectroscopy (XPS).

2. Experimental Methodology

2.1. Materials

In the current investigation, the martensitic and semi-austenitic PHSS steels were employed and tested in the as-received condition. The nominal chemical composition of these PHSS [47,48] is shown in Table 1.

PHSS samples were prepared by metallography (grinding and polishing employed 400, 500, 600, and 800 grade SiC sandpaper) and, subsequently, cleaned for 10 min using ultrasonic in ethanol and deionized water [49].

Table 1. Chemical composition of the martensitic and semi-austenitic precipitation hardening stainless steel (wt.%).

PHSS	Elements											
	Cr	Ni	Mo	Mn	Cu	Ti	Nb	N	Si	S	C	Fe
Martensitic	14.0–16.0	5.0–7.0	0.50–1.0	1.00	1.25–1.75	0.90–1.40	0.5–0.75	≤0.1	1.00	0.030	≤0.05	Balance
Semi-austenitic	16.0–17.0	4.0–5.0	2.50–3.25	0.50–1.25	–	–	–	0.07–0.13	≤0.50	0.030	0.07–0.11	Balance

2.2. Passivation Treatment

The passivation treatment followed the specification ASTM A967-17 [21] and ASTM A380-17 [50], which regulated the stages of pretreatment, passivation, time, temperature and final treatment. See Figure 1.

A design of experiments 5 (DoE) was carried out; due to different combinations of acid solutions, applied with 3-factor; and 2-tier to obtain the optimal concentration, temperature, and passivation time in the baths.

Table 2 shows the passivation treatment parameters exposure for each type of PHSS.

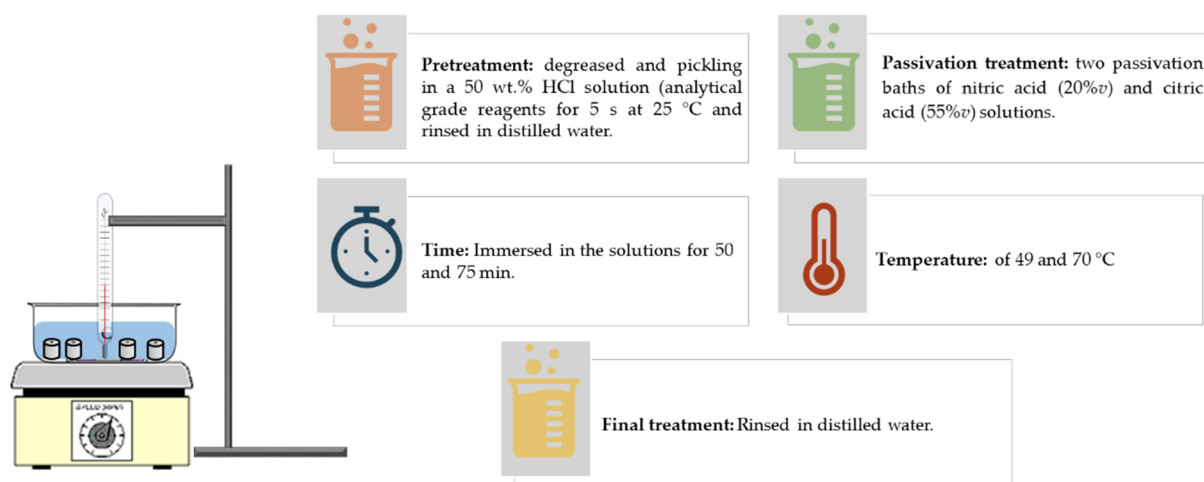


Figure 1. Diagram of passivation treatment of PHSS.

Table 2. Nomenclature and passivation treatment parameters.

PHSS	Passivation Baths	Time (min)	Temperature (°C)	Nomenclature Samples *
semi-austenitic	C ₆ H ₈ O ₇	50	49	semi-austenitic-CA-75 min-49 °C
	HNO ₃	50	70	semi-austenitic-NA-50 min-70 °C
	HNO ₃	50	70	semi-austenitic-NA-50 min-70 °C
	C ₆ H ₈ O ₇	75	49	semi-austenitic-CA-75 min-49 °C
martensitic	HNO ₃	75	70	martensitic-NA-75 min-70 °C
	HNO ₃	50	49	martensitic-NA-50 min-49 °C
	C ₆ H ₈ O ₇	50	49	martensitic-CA-50 min-49 °C
	C ₆ H ₈ O ₇	75	49	martensitic-CA-75 min-49 °C

* Citric acid (CA) and nitric acid (NA).

2.3. Microstructural Characterization

Optical microscopy (OM, Olympus, Hamburg, Germany) was used to determine the microstructure of PHSS; while the micrographs were taken by scanning electron microscopy (SEM, JEOL-JSM-5610LV, Tokyo, Japan) using a secondary electrons (SE) detector at 500×, operating at 20 kV, WD = 14 mm.

2.4. Corrosion Test

Corrosion measurements were conducted at room temperature using an electrochemical interface mod. 1287A—Solartron (Bognor Regis, UK) two 5 wt.% NaCl and 1 wt.% H₂SO₄ solutions [5,6]. The corrosion cell configuration consisted of a working electrode, WE (material to study), a reference electrode of saturated calomel (SCE), and a platinum mesh that served as a counter electrode (CE) for the current measurements [6,51,52]. The potentiodynamic polarization (PP) parameters regarding the potential scan range were applied between −1.0 and 1.0 V from OCP and a sweep rate of 0.06 V/min, according to ASTM G5-11 [50,53]. Tests were realized in triplicate.

2.5. XPS Characterization

High-resolution XPS analyses determined the oxide layer's surface chemical composition and valence states in the martensitic and semi-austenitic PHSS. A Thermo Fisher Scientific ESCALAB 250 Xi equipment (Waltham, MA, USA) was operated at a pressure of 10 mBar; the analysis conditions for the high-resolution zones and analysis radius of μm, (eV step energy, 45° of “take-off angle” with 0.1 eV step), and the excitation of the analyzed photoelectrons were measured with a monochromatic Al KAlpha X-ray source (1486 eV).

3. Results and Discussion

3.1. OM-SEM Microstructural

OM and SEM techniques were applied to study the microstructures of the samples in initial conditions. Figure 2 shows the martensitic and semi-austenitic PHSS micrographs (a, b) OM and (a', b') SEM-SE. The martensitic PHSS shows a martensitic (α') phase, and semi-austenitic PHSS contains a microstructure of austenite (γ) and delta (δ) ferrite phase, respectively. The SEM analysis corroborates the results. The presence of austenite (γ) in semi-austenitic steels is a thermodynamically stable phase, where an aging treatment can transform this phase. Likewise, alloying elements were found to indicate the presence of the delta ferrite (δ) phase [54–56].

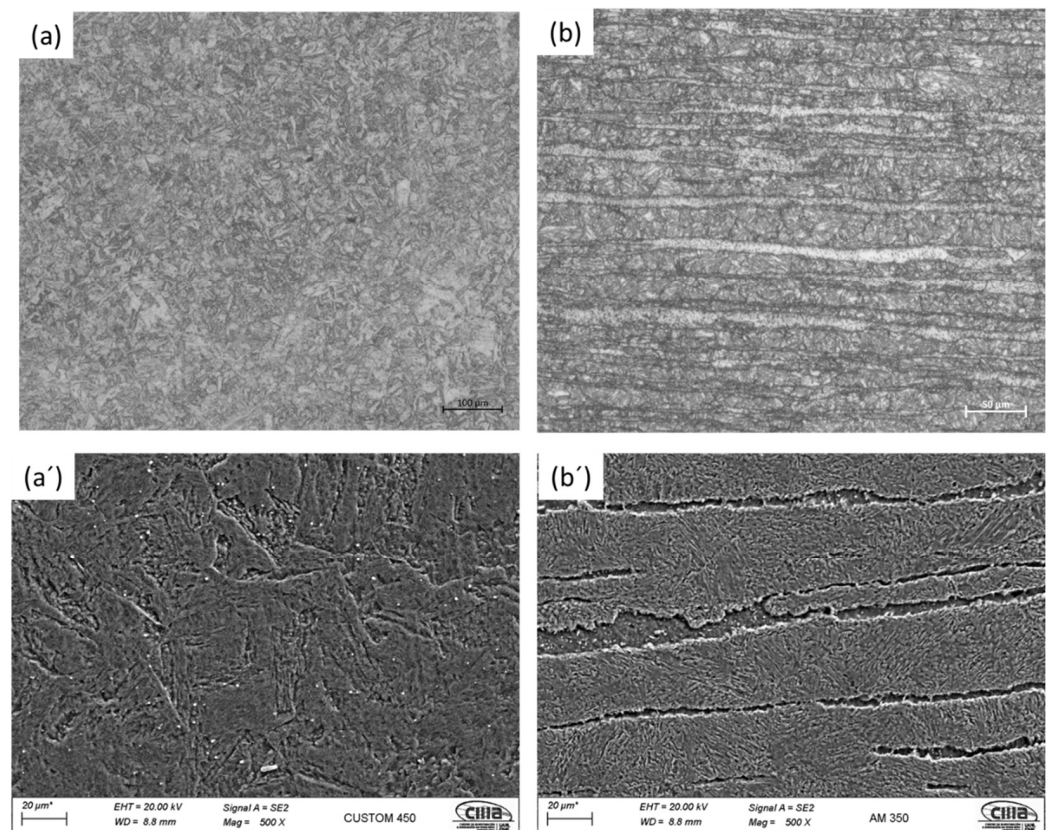


Figure 2. Microstructure of martensitic and semi-austenitic precipitation hardening stainless steel (initial conditions): (a,b) OM; (a',b') SEM-SE.

The martensitic stainless steels have higher carbon contents than most that are semi-austenitic. This reduces the corrosion resistance but increases mechanical properties such as toughness and increases the susceptibility to chromium carbide precipitation at grain boundaries.

The pitting corrosion is often measured using the pitting resistance equivalent number (PREN). From this theoretical standpoint, and based on their chemical compositions, the pitting corrosion resistance of various grades of stainless steels can be compared [57,58]. High PREN values indicate higher corrosion resistance (see Table 3). The PREN is determined by the alloying elements such as chromium, molybdenum, and nitrogen contents, and the most commonly used version of the Equation (1) is:

$$\text{PREN} = \text{Cr} + 3.3\text{Mo} + 16\text{N} \quad (1)$$

Table 3. Pitting resistance equivalent numbers of the martensitic and semi-austenitic precipitation hardening stainless steel.

PHSS	Cr	Mo	N	PREN
Martensitic	14.0–16.0	0.50–1.0	≤0.1	17.26
Semi-austenitic	16.0–17.0	2.50–3.25	0.07–0.13	25.37

3.2. Corrosion Test

Potentiodynamic Polarization

The corrosion behavior was observed by using potentiodynamic polarization. The Tafel extrapolation of PP was employed to determine the corrosion current density, i_{corr} ($\mu\text{A}\cdot\text{cm}^{-2}$), potential corrosion, E_{corr} (V), and corrosion rate [5,59–62]. The presence of a linear section in the potentiodynamic polarization curve is necessary for using the Tafel extrapolation method. A range of ± 300 mV on E_{corr} was determined to be in the linear section of at least one decade of current [63–65]. The PP obtained for the martensitic and semi-austenitic PHSS passivated in acid baths at 49 and 70 °C for 50 and 75 min and immersed in 5 wt.% NaCl and 1 wt.% H_2SO_4 solutions are shown in Figures 3 and 4.

The results for PHSS immersed in NaCl solution shows that the active E_{corr} (-0.384 V) value was recorded for the Martensitic-CA-50 min-49 °C, while the Semi-austenitic-NA-50 min-70 °C and Martensitic-NA-75 min-70 °C samples have the highest E_{corr} (both -0.234 V). Pitting potentials (E_{pitt}) have values from 0.401 up to 0.934 V. The semi-austenitic-NA-50 min-70 °C showed the best behavior of the nitric acid passivation treatment, which was corroborated by the lower corrosion rate (2.55×10^{-4} mm/yr) obtained. The passivation (range of 0.638 to 1.119 V) showed just a trend in PHSS steels since it was not fully defined.

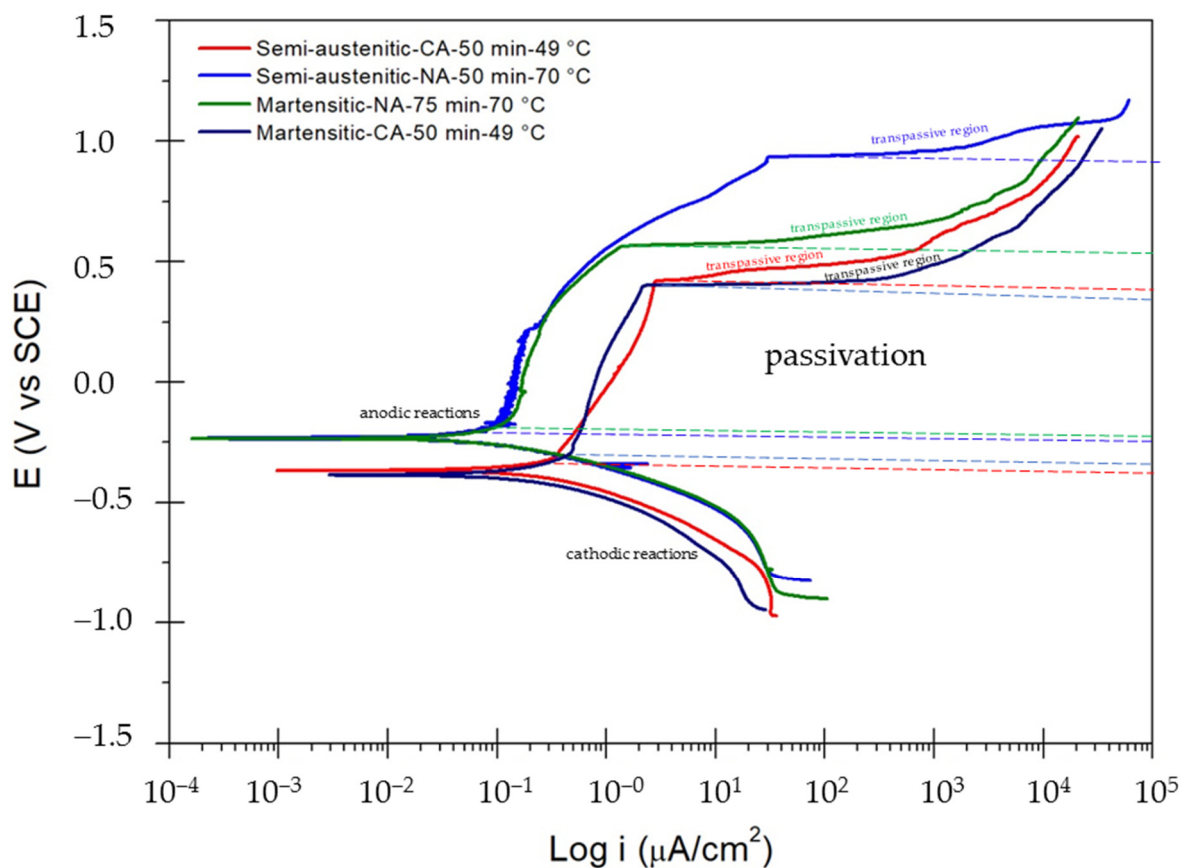
**Figure 3.** Potentiodynamic polarization curves for passivated martensitic and semi-austenitic PHSS in 5 wt.% NaCl solution.

Figure 4 shows the results for PHSS immersed in H_2SO_4 . The corrosion potentials (E_{corr}) were found in the range of -0.266 and -0.349 V, respectively. Pitting potential (E_{pitt}) values were observed from 0.766 up to 0.875 V. All steels under study had a higher and more defined passivation range (0.692 to 1.055 V) than the samples immersed in NaCl. The corrosion rates are higher ($\times 10^{-2}$ mm/yr) except for the semi-austenitic-NA-50 min-70 °C sample that presented a low corrosion rate (3.62×10^{-4} mm/yr).

Tables 4 and 5 show the electrochemical parameters obtained by potentiodynamic polarization (PP) curves. High values of corrosion rates in PHSS immersed in 5 wt.% NaCl solution (within the same order of magnitude) were recorded for nitric acid ($\times 10^{-4}$ mm/yr) and citric acid ($\times 10^{-3}$ mm/yr) passivation. Low values of corrosion rate in PHSS immersed in 1 wt.% H_2SO_4 solution (in the order of $\times 10^{-2}$ mm/yr) were recorded, except for the semi-austenitic-NA-50 min-70 °C sample, which presented a low corrosion rate (3.62×10^{-4} mm/yr). Passivation current and i_{pass} , values are higher for samples exposed to sulfuric acid, ranging from 0.506 up to $9.837 \mu A \cdot cm^{-2}$.

Table 4. Parameters obtained by PP for passivated martensitic and semi-austenitic. PHSS in 5 wt.% NaCl solution.

Sample	E_{corr} (Volts)	E_{pitt} (Volts)	i_{corr} ($\mu A \cdot cm^{-2}$)	i_{pass} ($\mu A \cdot cm^{-2}$)	Range Passive (Volts)	CR (mm/yr)
Semi-austenitic-CA-50 min-49 °C	-0.365	0.422	7.82×10^{-1}	0.352	0.736	1.26×10^{-3}
Semi-austenitic-NA-50 min-70 °C	-0.234	0.934	1.58×10^{-1}	0.082	1.119	2.55×10^{-4}
Martensitic-NA-75 min-70 °C	-0.234	0.565	1.37×10^{-1}	0.119	0.740	2.25×10^{-4}
Martensitic-CA-50 min-49 °C	-0.384	0.401	3.44×10^{-1}	0.480	0.688	5.65×10^{-3}

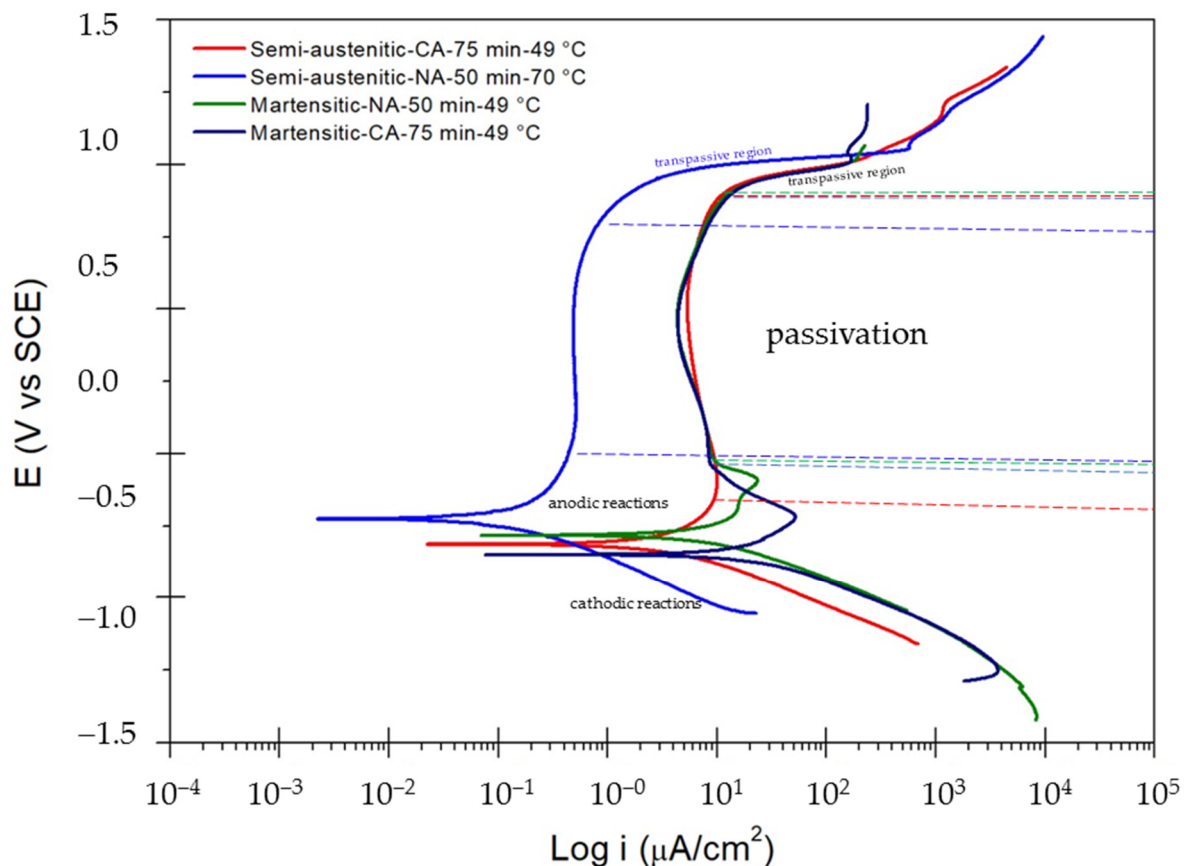


Figure 4. Potentiodynamic polarization curves for passivated martensitic and semi-austenitic. PHSS in 1 wt.% H_2SO_4 solution.

Table 5. Parameters obtained by PP for passivated martensitic and semi-austenitic. PHSS in 1 wt.% H₂SO₄ solution.

Sample	E _{corr} (Volts)	E _{pitt} (Volts)	i _{corr} (μA·cm ⁻²)	i _{pass} (μA·cm ⁻²)	Range passive (Volts)	CR (mm/yr)
Semi-austenitic-CA-75 min-49 °C	-0.314	0.875	0.7 × 10 ⁻¹	9.837	1.055	1.13 × 10 ⁻²
Semi-austenitic-NA-50 min-70 °C	-0.226	0.766	2.24 × 10 ⁻¹	0.506	0.692	3.62 × 10 ⁻⁴
Martensitic-NA-50 min-49 °C	-0.282	0.898	2.25 × 10 ⁻¹	8.529	0.899	3.69 × 10 ⁻²
Martensitic-CA-75 min-49 °C	-0.349	0.857	5.37 × 10 ⁻¹	8.193	0.880	8.82 × 10 ⁻²

The current results indicate that all systems showed a mixed activation and passivation followed by a transpassivation or secondary passivation trend.

Cheng et al. [66] stated that stainless steels commonly have primary and secondary passive films formed before and after transpassivation. When the passivated material begins to dissolve, the electrode potential is too noble (positive values). This represents a corrosion mechanism called transpassivation [5,6]. Studies on the formation of passive stainless-steel films have focused on the main passive region but not on the second film [28,67–76].

The PP curves show passivation behavior for the martensitic and semi-austenitic PHSS in acid solutions. The dissolution of the passive layer in the anodic region is the start of the transpassivation region [77–79]. The chromium oxidation transforms the primary passive film into a second passive film [80–82]. The film growth period involves iron and chromium oxidation [5,6,83–87].

The transpassive region is above 300 mV vs. ECS for samples in NaCl solution and is above 0.700 V for samples in H₂SO₄ solution. The passive film formed with nitric and citric acid baths at longer times has higher passivation ranges in H₂SO₄ than in NaCl solution.

3.3. XPS Analysis

XPS measurements determine the valence states, oxide layer composition, and surface chemical in the passivated martensitic and semi-austenitic PHSS, as shown in Figures 5–11.

XPS analysis was conducted with the Avantage software (Waltham, MA, USA). The NIST database (National Institute of Standards and Technology; Gaithersburg, MD, USA) was used to perform the deconvolution calculations of the XPS spectra and assign the chemical compounds through the binding energy peaks.

High-resolution XPS spectra are shown in Figures 5–11, obtained for Cr 2p and O 1s. In XPS spectra for Cr 2p, four chemical compounds were found: Cr₂O₃, Cr₇C₃, CrO₃ and Cr(C₆H₆)₂, as shown in Figures 5a, 6a, 7a, 8a, 9a, 10a and 11a. According to the literature [88–90], the Cr₂O₃ presence corresponding to the passive layer composition can be found from 576 to 578 eV; the obtained binding energy peaks ranged from 576.69 to 577.07 eV, according to the values reported for the chromium oxide layers. Finally, Figures 5a', 6a', 7a', 8a', 9a', 10a' and 11a' summarize the parameters obtained from full width at half maximum (FWHM) fitting, area ratio, and the peak binding energy, respectively.

In XPS spectra, the contributions of O 1s indicate binding energies for O 1s, from 532.23 to 532.94 eV according to the Gauss–Lorentz peak (see Figures 5b', 6b', 7b', 8b', 9b', 10b' and 11b'). Five chemical species were found Cr₂O₃, Fe(OH)O, Fe₂O₃, SiO₂ y Cr(OH)₃. Natajara et al. [91] indicated that the presence of oxides gives rise to chrome hydroxides and oxide formation on the surface due to OH⁻. The binding energy peaks obtained for Fe(OH)O and Fe₂O₃ ranged from 530.26 to 531.08 eV and 528.9 to 531.8 eV, respectively.

The detection of silicon oxide (SiO₂) in the high-resolution XPS spectra of the O 1s orbital, whose binding energy is between 532.23 and 532.94 eV, Figures 5b', 7b' and 11b', can be attributed to polishing or impurities in the passivating solutions. In the literature, different species have been found in the oxides generated by the passivation treatment of aged solutions [40,92].

According to the literature, the formation of the chromium oxide layer increases corrosion resistance thanks to the anticorrosive properties provided by chromium oxide.

The analysis of the O 1s contributions in most of the deconvolutions shows different Fe oxides and hydroxides, mainly associated with Fe^{3+} . The contributions by Cr 2p show the main peak around 576 eV. As the XPS spectra appear with an inclination at an energy value above 577 eV, the appearance of hydroxide and trioxide species will be more frequent. When analyzing Cr 2p, however, the main peaks were found at an energy level of 576 eV, presumably due to the chromium oxide layer derived from the passivation process.

According to Jung and Mesquita [92,93], there is a relationship between Fe oxides, hydroxides, and Cr oxides. The more Fe is dissolved during the passivation process, the more chromium oxides tend to enrich the passive layer, increasing the corrosion resistance.

Previous studies have revealed that passive films have a bilayer structure [94–96]. The compact inner layer is mainly composed of chromium(III) oxide, while the porous outer layer is mainly composed of iron and chromium oxides and hydroxides.

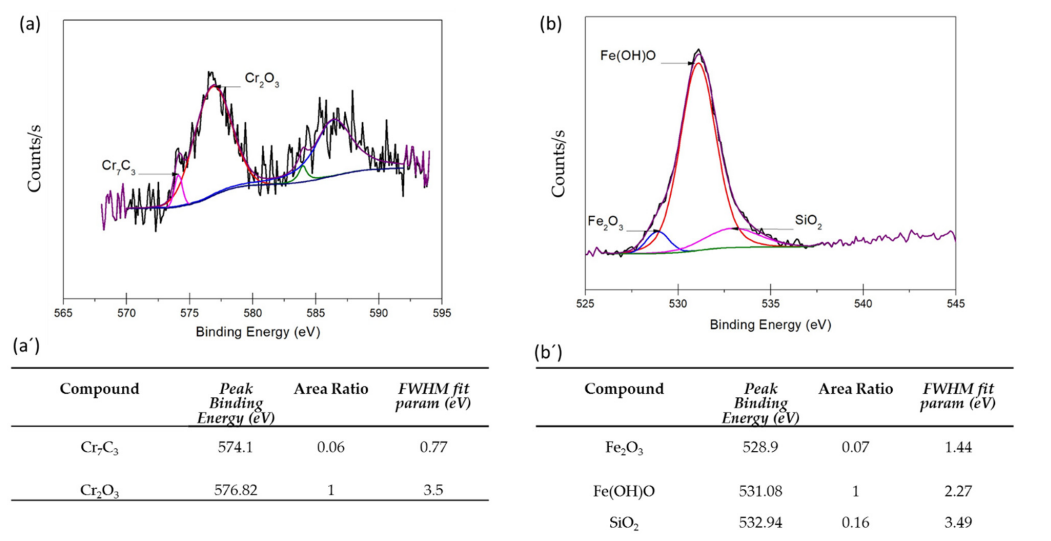


Figure 5. X-ray photoelectron spectra for AM350CA–50 min–49 °C: (a) Cr 2p, (b) O 1s. Parameters obtained: peak binding energy and FWHM fit param (a') Cr 2p, (b') O 1s.

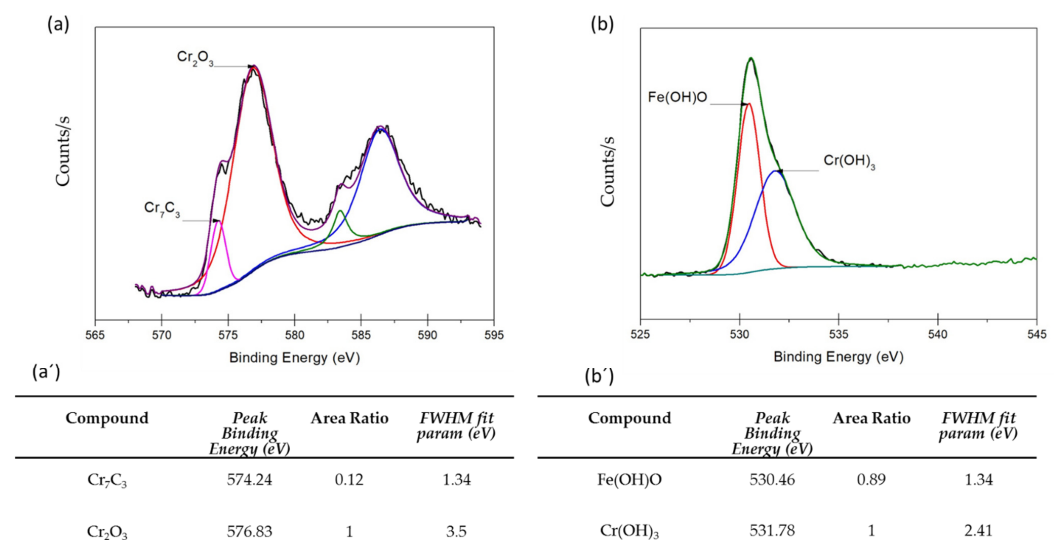


Figure 6. X-ray photoelectron spectra for CUSTOM450NA–75 min–70 °C: (a) Cr 2p, (b) O 1s. Parameters obtained: peak binding energy and FWHM fit param (a') Cr 2p, (b') O 1s.

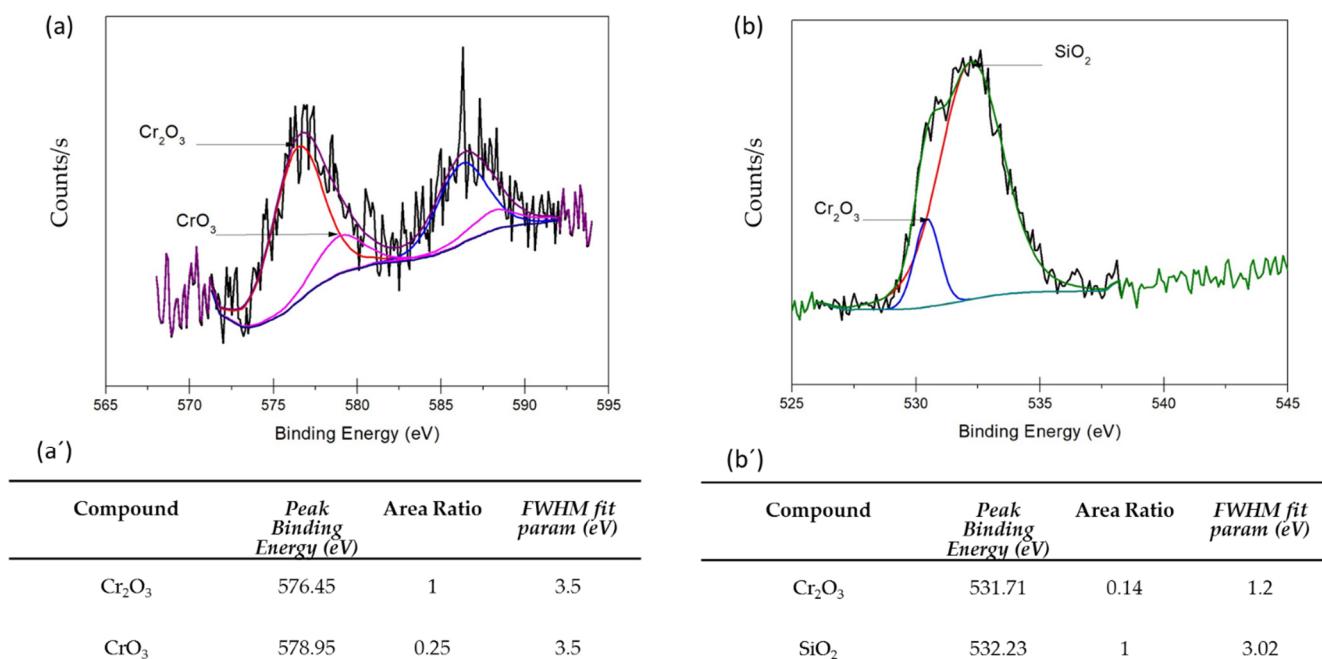


Figure 7. X-ray photoelectron spectra for CUSTOM 450CA–50 min–49 °C: (a) Cr 2p, (b) O 1s. Parameters obtained: peak binding energy and FWHM fit param (a') Cr 2p, (b') O 1s.

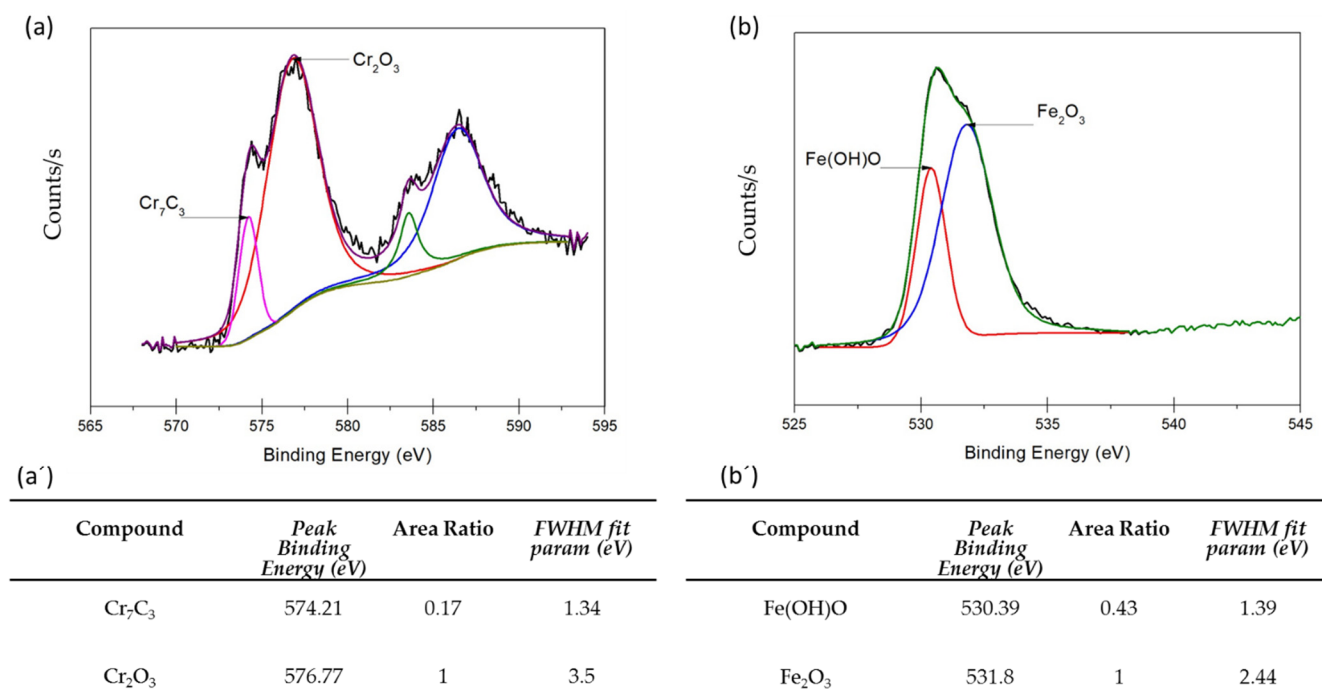


Figure 8. X-ray photoelectron spectra for AM350CA–75 min–49 °C: (a) Cr 2p, (b) O 1s. Parameters obtained: peak binding energy and FWHM fit param (a') Cr 2p, (b') O 1s.

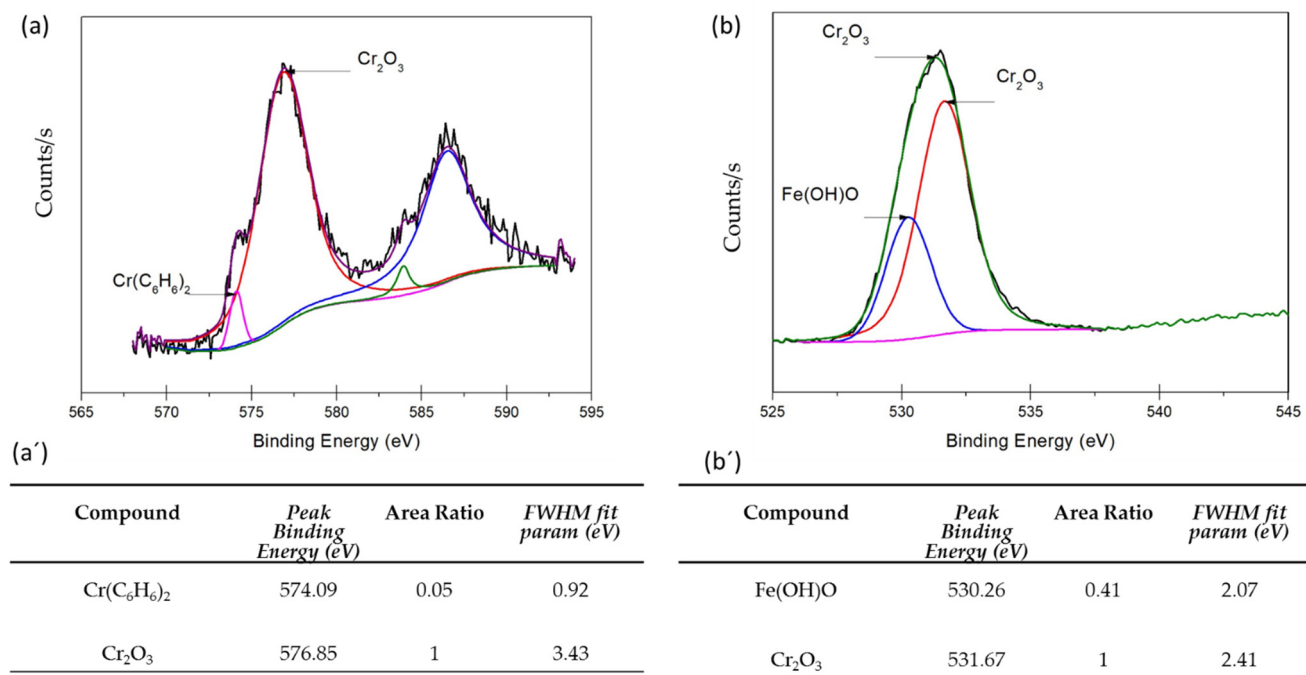


Figure 9. X-ray photoelectron spectra for AM350NA–50 min–70 °C: (a) Cr 2p, (b) O 1s. Parameters obtained: peak binding energy and FWHM fit param (a') Cr 2p, (b') O 1s.

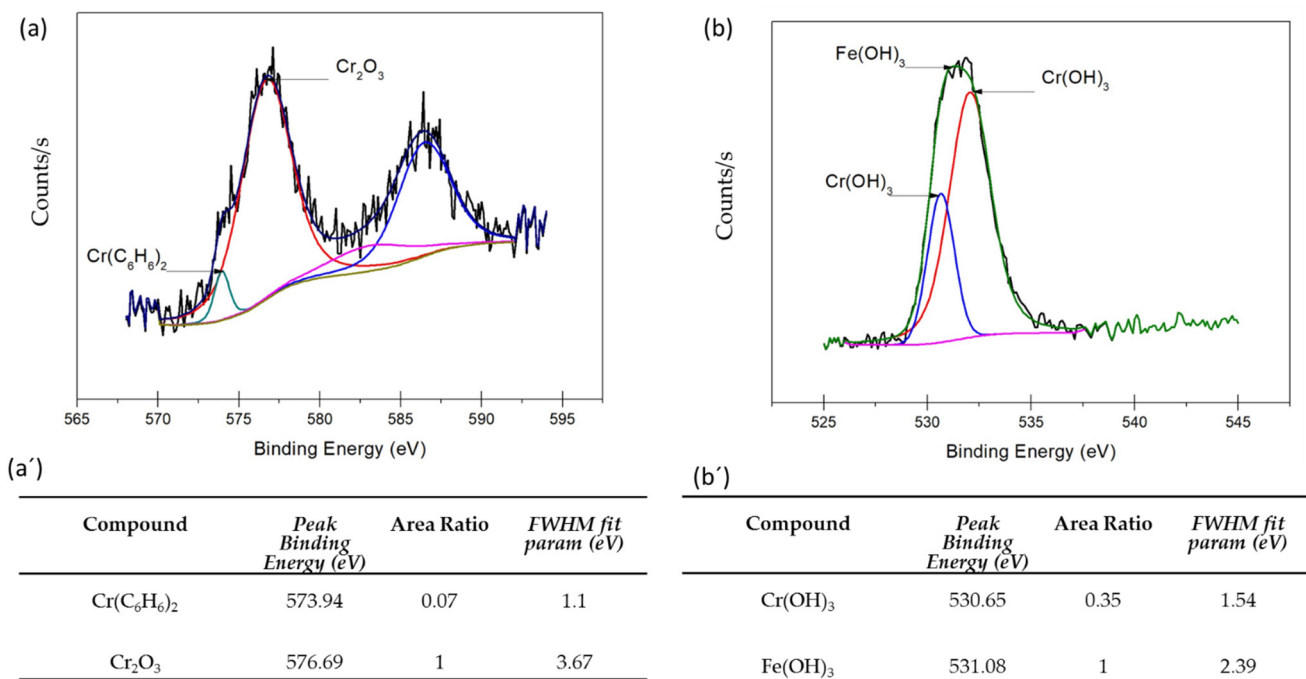


Figure 10. X-ray photoelectron spectra for CUSTOM450NA–50 min–49 °C: (a) Cr 2p, (b) O 1s. Parameters obtained: peak binding energy and FWHM fit param (a') Cr 2p, (b') O 1s.

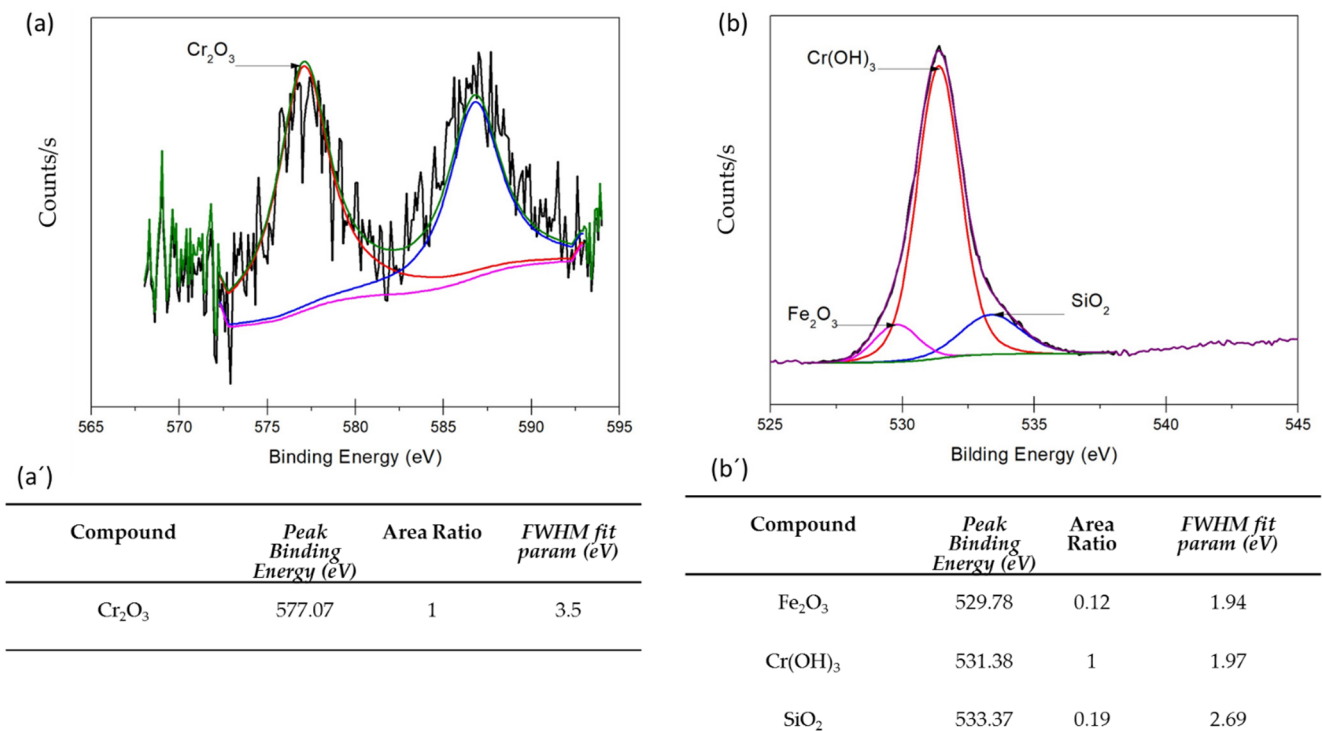


Figure 11. X-ray photoelectron spectra for CUSTOM450CA-75 min-49 °C: (a) Cr 2p, (b) O 1s. Parameters obtained: peak binding energy and FWHM fit param (a') Cr 2p, (b') O 1s.

4. Conclusions

This work studies the passive state of martensitic and semi-austenitic PHSS passivated in citric and nitric acid baths at 49 and 70 °C for 50 and 75 min and immersed in 5 wt.% NaCl and 1 wt.% H₂SO₄ solutions. From the current experimental results, it can be concluded the following:

- OM-SEM characterization indicated that the martensitic PHSS presented a microstructure with a martensitic (α') phase and a semi-austenitic PHSS containing a microstructure of austenite (γ) and delta (δ) ferrite phases, respectively. Based on the values obtained from PREN, the semi-austenitic PHSS (25.37) presented a higher corrosion resistance than the martensitic PHSS (17.26).
- Potentiodynamic polarization results indicated that martensitic and semi-austenitic steels passivated in nitric acid showed lower corrosion resistance values (in the order of $\times 10^{-4}$ mm/yr).
- Nitric acid passivation made the surface susceptible to localized corrosion. The potentiodynamic polarization curves for PHSS immersed in 5 wt.% NaCl solution indicated that the passivation showed a trend since it is not fully defined.
- Despite having a well-defined passivation layer, passive samples studied in H₂SO₄ solution presented an increase in corrosion kinetics.
- Passivation current, i_{pass} , was found to have higher values for samples exposed to sulfuric acid (from 0.506 up to 9.837 $\mu\text{A}\cdot\text{cm}^{-2}$).
- XPS analysis determined that the different chemical species on the surface film of martensitic and semi-austenitic PHSS in this work included Cr₂O₃ and Fe(OH)O. Passive films contained iron and chromium oxide and hydroxide.
- The samples passivated at 70 °C are the ones that presented the best results independently of the steel, passivating solution, and time.
- The citric acid passivation process on PHSS could be a green alternative to the currently employed nitric acid passivation process.

Author Contributions: Conceptualization, F.A.-C., O.S.-G. and C.G.-T.; methodology, O.S.-G., J.O.-C., J.P.F.-D.I.R., R.G.B.-M. and E.M.-B., data curation, F.A.-C., J.C.-M., C.G.-T.; J.M.J.-M. and D.N.-M. formal analysis, O.S.-G., F.A.-C. and C.G.-T. writing—review and editing, F.A.-C., O.S.-G., R.G.B.-M. and C.G.-T. All authors have read and agreed to the published version of the manuscript.

Funding: This research was funded by the Mexican National Council for Science and Technology (CONACYT) through projects A1-S-8882 and Universidad Autónoma de Nuevo León (UANL).

Institutional Review Board Statement: Not applicable.

Informed Consent Statement: Not applicable.

Data Availability Statement: The data presented in this study are available on request from the corresponding author.

Acknowledgments: The authors wish to thank the Academic Body UANL—CA-316 “Deterioration and integrity of composite materials” and the technical assistance from M. Sc. Luis G. Silva Vidaurri.

Conflicts of Interest: The authors declare no conflict of interest.

References

1. Gialanella, S.; Malandrucolo, A. Aerospace Alloys. In *Topics in Mining, Metallurgy and Materials Engineering*; Bergmann, C.P., Ed.; Springer: Cham, Switzerland, 2020; ISSN 2364-3307. [\[CrossRef\]](#)
2. Mouritz, P.A. *Introduction to Aerospace Materials*; Woodhead Publishing: Cambridge, UK, 2012.
3. Gloria, A.; Montanari, R.; Richetta, M.; Varone, A. Alloys for aeronautic applications: State of the art and perspectives. *Metals* **2019**, *9*, 662. [\[CrossRef\]](#)
4. Cabral-Miramontes, J.A.; Barceinas-Sánchez, J.D.O.; Poblano-Salas, C.A.; Pedraza-Basulto, G.K.; Nieves-Mendoza, D.; Zambrano-Robledo, P.C.; Almeraya-Calderón, F.; Chacón-Nava, J.G. Corrosion behavior of AISI 409Nb stainless steel manufactured by powder metallurgy exposed in H₂SO₄ and NaCl solutions. *Int. J. Electrochem. Sci.* **2013**, *8*, 564–577.
5. Lara-Banda, M.; Gaona-Tiburcio, C.; Zambrano-Robledo, P.; Delgado, -E.M.; Cabral-Miramontes, J.A.; Nieves-Mendoza, D.; Maldonado-Bandala, E.; Estupiñán-López, F.; Chacón-Nava, J.G.; Almeraya-Calderón, F. Alternative to nitric acid passivation of 15-5 and 17-4PH stainless steel using electrochemical techniques. *Materials* **2020**, *13*, 2836. [\[CrossRef\]](#) [\[PubMed\]](#)
6. Lara Banda, M.; Gaona-Tiburcio, C.; Zambrano-Robledo, P.; Cabral, M.J.A.; Estupinan, F.; Baltazar-Zamora, M.A.; Almeraya-Calderon, F. Corrosion Behaviour of 304 Austenitic, 15–5PH and 17-4PH Passive Stainless Steels in acid solutions. *Int. J. Electrochem. Sci.* **2018**, *13*, 10314–10324. [\[CrossRef\]](#)
7. Lopes, J.C. Material selection for aeronautical structural application. *Sci. Technol. Adv. Mat.* **2008**, *20*, 78–82.
8. Lo, K.H.; Shek, C.H.; Lai, J.K.L. Recent developments in stainless steels. *Mater. Sci. Eng. R* **2009**, *65*, 39–104. [\[CrossRef\]](#)
9. Mortezaei, S.; Arabi, H.; Seyedein, H.; Momeny, A.; Soltanlinezhad, M. Investigation on Microstructure Evolution of a Semi-Austenitic Stainless Steel Through Hot Deformation. *Iran. J. Mater. Sci. Eng.* **2020**, *17*, 60–90. [\[CrossRef\]](#)
10. Ha, H.Y.; Jang, J.H.; Lee, T.H.; Won, C.; Lee, C.H.; Moon, J.; Lee, C.G. Investigation of the localized corrosion and passive behavior of type 304 stainless steels with 0.2–1.8 wt% B. *Materials* **2018**, *11*, 2097. [\[CrossRef\]](#)
11. Abdelshehid, M.; Mahmodieh, K.; Mori, K.; Chen, L.; Stoyanov, P.; Davlantes, D.; Foyos, J.; Ogren, J.; Clark, R., Jr.; Es-Said, O.S. On the correlation between fracture toughness and precipitation hardening heat treatments in 15-5PH stainless steel. *Eng. Fail. Anal.* **2007**, *14*, 626–631. [\[CrossRef\]](#)
12. Esfandiari, M.; Dong, H. The corrosion and corrosion–wear behaviour of plasma nitrided 17-4PH precipitation hardening stainless steel. *Surf. Coat. Technol.* **2007**, *202*, 466–478. [\[CrossRef\]](#)
13. Dong, H.; Esfandiari, M.; Li, X.Y. On the microstructure and phase identification of plasma nitrided 17-4PH precipitation hardening stainless steel. *Surf. Coat. Technol.* **2008**, *202*, 2969–2975. [\[CrossRef\]](#)
14. Hsiao, C.N.; Chiou, C.S.; Yang, J.R. Aging reactions in a 17-4 PH stainless steel. *Mater. Chem. Phys.* **2002**, *74*, 134–142. [\[CrossRef\]](#)
15. Gladman, T. Precipitation hardening in metals. *Mater. Sci. Technol.* **1999**, *15*, 30–36. [\[CrossRef\]](#)
16. Schade, C.; Stears, P.; Lawley, A.; Doherty, R. Precipitation Hardening PM Stainless Steels. *Int. J. Powder Metall.* **2006**, *1*, 51–59.
17. Cobb, H.M. *The History of Stainless Steel*; ASM International: Geauga, OH, USA, 2010.
18. Farrar, J. *The Alloy Tree—A Guide to Low-Alloy Steels, Stainless Steels and Nickel-Base Alloys*; Woodhead Publishing Limited and CRC Press: Sawston, UK, 2004.
19. Baltazar, M.A.; Bastidas, D.M.; Santiago, G.; Mendoza, J.M.; Gaona, C.; Bastidas, J.M.; Almeraya, F. Effect of silica fume and fly ash admixtures on the corrosion behavior of AISI 304 embedded in concrete exposed in 3.5% NaCl solution. *Materials* **2019**, *12*, 4007. [\[CrossRef\]](#)
20. Schmuki, P. From bacon to barriers: A review on the passivity of metal and alloys. *J. Solid. State Electr.* **2002**, *6*, 145–164. [\[CrossRef\]](#)
21. ASTM A967-17; Standard Specification for Chemical Passivation Treatments for Stainless Steel Parts. ASTM International: West Conshohocken, PA, USA, 1999.
22. Shibata, T. Stochastic studies of passivity breakdown. *Corros. Sci.* **1990**, *31*, 413–423. [\[CrossRef\]](#)

23. Ashassi-Sorkhabi, H.; Seifzadeh, D.; Raghbi-Boroujeni, M. Analysis of electrochemical noise data in both time and frequency domains to evaluate the effect of ZnO nanopowder addition on the corrosion protection performance of epoxy coatings. *Arab. J. Chem.* **2016**, *9*, S1320–S1327. [CrossRef]
24. Isselin, J.; Kasada, R.; Kimura, A. Effects of aluminum on the corrosion behavior of 16% Cr ODS ferritic steels in a nitric acid solution. *J. Nucl. Sci. Technol.* **2011**, *48*, 169–171. [CrossRef]
25. Martínez-Villafaña, A.; Almeraya-Calderón, M.F.; Gaona-Tiburcio, C.; Gonzalez-Rodriguez, J.G.; Porcayo-Calderón, J. High-Temperature Degradation and Protection of Ferritic and Austenitic Steels in Steam Generators. *J. Mater. Eng. Perform.* **1998**, *7*, 108–113. [CrossRef]
26. Lewis, P.; Kolody, M. Alternative to Nitric Acid Passivation of Stainless Steel Alloys. In *Technology Evaluation for Environmental Risk Mitigation Compendium, Proceedings of the NASA Technology Evaluation for Environmental Risk Mitigation Principal Center (TEERM)*; Department of Defense (DoD) and NASA, Kennedy Space Center: Merritt Island, FL, USA, 2008.
27. Yasensky, D.; Reali, J.; Larson, C.; Carl, C. Citric acid passivation of stainless steel. In Proceedings of the Aircraft Airworthiness and Sustainment Conference, San Diego, CA, USA, 18–21 April 2009.
28. Gaydos, S.P. Passivation of aerospace stainless parts with citric acid solutions. *Plat. Surf. Finish.* **2003**, *90*, 20–25.
29. Suresh, G.U.; Kamachi, M.S. Electrochemical Noise Analysis of Pitting Corrosion of Type 304L Stainless Steel. *Corrosion* **2014**, *70*, 283–293. [CrossRef]
30. Montoya-Rangel, M.; de Garza-Montes, O.N.; Gaona-Tiburcio, C.; Colás, R.; Cabral-Miramontes, J.; Nieves-Mendoza, D.; Maldonado-Bandala, E.; Chacón-Nava, J.; Almeraya-Calderón, F. Electrochemical Noise Measurements of Advanced High-Strength Steels in Different Solutions. *Metals* **2020**, *10*, 1232. [CrossRef]
31. Bragaglia, M.; Cherubini, V.; Cacciotti, I.; Rinaldi, M.; Mori, S.; Soltani, P.; Nanni, F.; Kaciulis, S.; Montesperelli, G. Citric Acid Aerospace Stainless Steel Passivation: A Green Approach. In Proceedings of the CEAS Aerospace Europe Conference 2015, Delft, The Netherlands, 7–11 September 2015.
32. Marcelin, S.; Pébèrea, N.; Régnier, S. Electrochemical characterisation of a martensitic stainless steel in a neutral chloride solution. *Electrochim. Acta* **2013**, *87*, 32–40. [CrossRef]
33. El-Taib Heakal, F.; Ghoneim, A.; Fekry, A. Stability of spontaneous passive films on high strength Mo-containing stainless steels in aqueous solutions. *J. Appl. Electrochem.* **2007**, *37*, 405–413. [CrossRef]
34. Ameer, M.A.; Fekry, A.M.; El-Taib Heakal, F. Electrochemical behaviour of passive films on molybdenum-containing austenitic stainless steels in aqueous solutions. *Electrochim. Acta* **2007**, *50*, 43–49. [CrossRef]
35. El-Taib Heakal, F.; Ameer, M.A.; El-Aziz, A.M.; Fekry, A.M. Electrochemical behavior of Mo-containing austenitic stainless steel in buffer solutions. *Mater. Sci. Eng. Technol.* **2004**, *35*, 407–413. [CrossRef]
36. Tseng, K.H.; Chen, Y.C.; Chen, Y.C. Micro Plasma Arc Welding of AM 350 Precipitation Hardening Alloys. *Appl. Mech. Mater.* **2012**, *121*, 2681–2685. [CrossRef]
37. Shaikh, H.; George, G.; Khatak, H.S. Failure analysis of an AM 350 steel bellows. *Eng. Fail. Anal.* **2001**, *8*, 571–576. [CrossRef]
38. Fakić, B.; Čubela, D. Review of the Development of Research in the Design of Semi Austenitic Stainless Steel 17-7PH. In Proceedings of the 17th International Research/Expert Conference “Trends in the Development of Machinery and Associated Technology” TMT 2013, Istanbul, Turkey, 10–11 September 2013; pp. 113–116.
39. Warren, J.; Wei, D.Y. The low cycle fatigue behavior of the controlled transformation stainless steel alloy AM355 at 121, 204 and 315 °C. *Mater. Sci. Eng. A* **2008**, *475*, 148–156. [CrossRef]
40. Favor, R.J.; Deel, O.L.; Achbach, W.P. *Design Information on AM-350 Stainless Steel for Aircraft and Missiles*; Defense Metals Information Center, Battelle Memorial Institute: Columbus, OH, USA, 1961; Volume 156.
41. Kumar, T.S.; Ramanujam, R.; Vignesh, M.; Rohith, D.; Manoj, V.; Sankar, P.H. Comparative machining studies on custom 450 alloy with TiCN, TiAlN coated and uncoated carbide tools using Taguchi-Fuzzy logic approach. *Mater. Res. Express* **2019**, *6*, 066411. [CrossRef]
42. Bocchetta, P.; Chen, L.-Y.; Tardelli, J.D.C.; Reis, A.C.D.; Almeraya-Calderón, F.; Leo, P. Passive layers and corrosion resistance of biomedical Ti-6Al-4V and β -Ti alloys. *Coatings* **2021**, *11*, 487. [CrossRef]
43. Lin, C.K.; Tsai, W.J. Corrosion fatigue behaviour of a 15Cr-6Ni precipitation-hardening stainless steel in different tempers. *Fatigue Fract. Eng. Mater. Struct.* **2000**, *23*, 489–497. [CrossRef]
44. Mollapour, Y.; Poursaeidi, E. Experimental and numerical analysis of Pitting Corrosion in CUSTOM 450 Stainless Steel. *Eng. Fail. Anal.* **2021**, *128*, 105589. [CrossRef]
45. Lin, C.K.; Chu, C.C. Mean stress effects on low-cycle fatigue for a precipitation-hardening martensitic stainless steel in different tempers. *Fatigue Fract. Eng. Mater. Struct.* **2000**, *23*, 545–553. [CrossRef]
46. Samaniego-Gómez, O.; Almeraya-Calderón, F.; Chacón-Nava, J.; Maldonado-Bandala, E.; Nieves-Mendoza, D.; Flores-De los Rios, J.P.; Jáquez-Muñoz, J.M.; Delgado, A.D.; Gaona-Tiburcio, C. Corrosion Behavior of Passivated CUSTOM450 and AM350 Stainless Steels For Aeronautical Applications. *Metals* **2022**, *12*, 666. [CrossRef]
47. AM 350 Technical Data. Available online: <https://www.hightempmetals.com/techdata/hitempAM350data.php> (accessed on 30 April 2022).
48. Custom 450[®] Stainless Steel. Available online: <https://www.ulbrich.com/uploads/data-sheets/Custom-450-Stainless-Steel-Wire-UNS-S45000.pdf> (accessed on 30 April 2022).

49. ASTM E3-95; Standard Practice for Preparation of Metallographic Specimens. ASTM International: West Conshohocken, PA, USA, 1995.
50. ASTM A380-17; Standard Practice for Cleaning, Descaling and Passivation of Stainless-Steel Parts, Equipment, and Systems. ASTM International: West Conshohocken, PA, USA, 1999.
51. Olguin Coca, F.J.; Loya Tello, M.U.; Gaona-Tiburcio, C.; Romero, J.A.; Martínez-Villafañe, A.; Maldonado, B.E.; Almeraya-Calderón, F. Corrosion Fatigue of Road Bridges: A review. *Int. J. Electrochem. Sci.* **2011**, *6*, 3438–3451.
52. Samaniego-Gámez, P.; Almeraya-Calderón, F.; Martín, U.; Röss, J.; Gaona-Tiburcio, C.; Silva-Vidaurre, L.; Cabral-Miramontes, J.; Bastidas, J.M.; Chacón-Nava, J.G.; Bastidas, D.M. Efecto del tratamiento de sellado en el comportamiento frente a corrosión de la aleación anodizada de aluminio-litio AA2099. *Rev. Met.* **2020**, *56*, e180. [[CrossRef](#)]
53. ASTM G5-11; Standard Reference Test Method for Making Potentiostatic and Potentiodynamic Anodic Polarization Measurements. ASTM International: West Conshohocken, PA, USA, 2011.
54. Gupta, A.; Bhargava, A.K.; Tewari, R.; Tiwari, A.N. TEM studies of boron-modified 17Cr-7Ni precipitation-hardenable stainless steel via rapid solidification route. *Metal. Mater. Trans. A* **2013**, *44*, 4248–4256. [[CrossRef](#)]
55. Xu, X.L.; Yu, Z.W. Metallurgical analysis on a bending failed pump-shaft made of 17-7PH precipitation-hardening stainless steel. *J. Mater. Process. Technol.* **2008**, *198*, 254–259. [[CrossRef](#)]
56. Abedi, H.R.; Hanzaki, A.Z.; Haghdadi, N.; Hodgson, P.D. Substructure induced twinning in low density steel. *Scr. Mater.* **2017**, *128*, 69–73. [[CrossRef](#)]
57. The British Stainless Steel Association 2022. Available online: https://bssa.org.uk/bssa_articles/calculation-of-pren/ accesseddate (accessed on 2 June 2022).
58. Schweitzer, P. *Fundamentals of Metallic Corrosion: Atmospheric and Media Corrosion of Metals*; CRC Press Taylor & Francis Group: Boca Raton, FL, USA, 2007; ISBN 10:0-8493-8243-2.
59. Tafel, J. Über die Polarisation bei kathodischer Wasserstoffentwicklung. *Z. Phys. Chem.* **1905**, *50*, 641–712. [[CrossRef](#)]
60. Pellegrini-Cervantes, M.J.; Almeraya-Calderon, F.; Borunda-Terrazas, A.; Bautista-Margulis, R.G.; Chacón-Nava, J.G.; Fajardo-San-Miguel, G.; Almaral-Sanchez, J.L.; Barrios-Durstewitz, C.; Martínez-Villafañe, A. Corrosion Resistance, Porosity and Strength of lended Portland Cement Mortar Containing Rice Husk Ash and Nano-SiO₂. *Int. J. Electrochem. Sci.* **2013**, *8*, 10697–10710.
61. Butler, J.A.V. Studies in heterogeneous equilibria. Part II.—The kinetic interpretation on the Nernst theory of electromotive force. *Trans. Faraday Soc.* **1924**, *19*, 729–733. [[CrossRef](#)]
62. Jaquez-Muñoz, J.; Gaona-Tiburcio, C.; Lira-Martinez, A.; Zambrano-Robledo, P.; Maldonado-Bandala, E.; Samaniego-Gamez, O.; Nieves-Mendoza, D.; Olguin-Coca, J.; Estupiñán-Lopez, F.; Almeraya-Calderon, F. Susceptibility to pitting corrosion of Ti-CP2, Ti-6Al-2Sn-4Zr-2Mo, and Ti-6Al-4V alloys for aeronautical applications. *Metals* **2021**, *11*, 1002. [[CrossRef](#)]
63. Zeng, Y.; Kang, L.; Wu, Y.; Wan, S.; Liao, B.; Li, N.; Guo, X. Melamine modified carbon dots as high effective corrosion inhibitor for Q235 carbon steel in neutral 3.5 wt% NaCl solution. *J. Mol. Liq.* **2022**, *349*, 118108. [[CrossRef](#)]
64. Wan, S.; Zhan, T.; Chen, H.; Liao, B.; Guo, X. Kapok leaves extract and synergistic iodide as novel effective corrosion inhibitors for Q235 carbon steel in H₂SO₄ medium. *Ind. Crops Prod.* **2022**, *178*, 114649. [[CrossRef](#)]
65. Buchanan, A.R.; Stansbury, E.E. *Handbook of Environmental Degradation of Materials (Second Edition) Chapter 4—Electrochemical Corrosion*; Elsevier Inc.: Amsterdam, The Netherlands, 2012; Volume 1, pp. 87–125. [[CrossRef](#)]
66. Cheng, M.; Chaofang, D.; Zhongyu, C.; Kui, X. A comparative study of primary and secondary passive films formed on AM355 stainless steel in 0.1 M NaOH. *Appl. Surf. Sci.* **2018**, *427*, 763–773. [[CrossRef](#)]
67. Betova, I.; Bojinov, M.; Laitinen, T.; Mäkelä, K.; Pohjanne, P.; Saario, T. The transpassive dissolution mechanism of highly alloyed stainless steels: I. Experimental results and modelling procedure. *Corros. Sci.* **2002**, *44*, 2675–2697. [[CrossRef](#)]
68. Ye, W.; Li, Y.; Wang, F. The improvement of the corrosion resistance of 309stainless steel in the transpassive region by nano-crystallization. *Electrochim. Acta* **2009**, *54*, 1339–1349. [[CrossRef](#)]
69. Gaona-Tiburcio, C.; Almeraya-Calderón, F.; Chacon-Nava, J.; Matutes-Aquino, A.M.; Martínez-Villafañe, A. Electrochemical response of permanent magnets in different solutions. *J. Alloys Compd.* **2004**, *369*, 78–80. [[CrossRef](#)]
70. Cabral-Miramontes, J.A.; Bastidas, M.D.; Baltazar, M.A.; Zambrano-Robledo, P.; Bastidas, J.M.; Almeraya-Calderón, F.; Gaona-Tiburcio, C. Corrosion behavior of Zn-TiO₂ and Zn-ZnO Electrodeposited Coatings in 3.5% NaCl solution. *Int. J. Electrochem. Sci.* **2019**, *14*, 4226–4239. [[CrossRef](#)]
71. Huang, J.; Wu, X.; Han, E.H. Electrochemical properties and growth mechanism of passive films on Alloy 690 in high-temperature alkaline environments. *Corros. Sci.* **2010**, *52*, 3444–3452. [[CrossRef](#)]
72. Calinski, C.; Strehblow, H.H. ISS depth profiles of the passive layer on Fe/Cr alloys. *J. Electrochem. Soc.* **1989**, *36*, 1328–1331. [[CrossRef](#)]
73. Gaona-Tiburcio, C.; Aguilar, L.M.R.; Zambrano-Robledo, P.; Estupiñán-López, F.; Cabral-Miramontes, J.A.; Nieves-Mendoza, D.; Castillo-González, E.; Almeraya-Calderón, F. Electrochemical Noise Analysis of Nickel Based Superalloys in Acid Solutions. *Int. J. Electrochem. Sci.* **2014**, *9*, 523–533.
74. Corral-Higuera, R.; Arredondo-Rea, P.; Neri-Flores, M.A.; Gómez-Soberón, J.M.; Almaral-Sánchez, J.L.; Castorena-González, J.C.; Almeraya-Calderón, F. Chloride ion penetrability and corrosion behavior of steel in concrete with sustainability characteristics. *Int. J. Electrochem. Sci.* **2011**, *6*, 958–970.
75. Núñez-Jaquez, R.E.; Buelna-Rodríguez, J.E.; Barrios-Durstewitz, C.P.; Gaona-Tiburcio, C.; Almeraya-Calderón, F. Corrosion of modified concrete with sugar cane bagasse ash. *Int. J. Corros.* **2012**, *2012*, 451864. [[CrossRef](#)]

76. Fattah-alhosseini, A.; Saatchi, A.; Golozar, M.A.; Raeissi, K. The transpassive dissolution mechanism of 316L stainless steel. *Electrochim. Acta* **2009**, *54*, 3645–3650. [[CrossRef](#)]
77. Macdonald, D.; Urquidi-Macdonald, M. Deterministic models for passivity breakdown. *Corros. Sci.* **1990**, *31*, 425–430. [[CrossRef](#)]
78. Macdonald, D.D. Point defect model for the passive state. *J. Electrochem. Soc.* **1992**, *139*, 3434–3449. [[CrossRef](#)]
79. Cui, Z.; Wang, L.; Ni, H.; Hao, W.; Man, C.; Chen, S.; Li, X. Influence of temperature on the electrochemical and passivation behavior of 2507 super duplex stainless steel in simulated desulfurized flue gas condensates. *Corros. Sci.* **2017**, *118*, 31–48. [[CrossRef](#)]
80. Bojinov, M.; Betova, I.; Fabricius, G.; Laitinen, T.; Saario, T. The stability of the passive state of iron–chromium alloys in sulphuric acid solution. *Corros. Sci.* **1999**, *41*, 1557–1584. [[CrossRef](#)]
81. Bojinov, M.; Fabricius, G.; Kinnunen, P.; Laitinen, T.; Mäkelä, K.; Saario, T.; Sundholm, G. The mechanism of transpassive dissolution of Ni–Cr alloys in sulphate solutions. *Electrochim. Acta* **2000**, *45*, 2791–2802. [[CrossRef](#)]
82. Maldonado-Bandala, E.E.; Jiménez-Quero, V.; Olguin-Coca, F.; Lizarraga, M.L.G.; Baltazar-Zamora, M.A.; Ortiz-C, A.; Almeraya, C.F.; Zambrano, R.P.; Gaona-Tiburcio, C. Electrochemical Characterization of Modified Concretes with Sugar Cane Bagasse Ash. *Int. J. Electrochem. Sci.* **2011**, *6*, 4915–4926.
83. Radhakrishnamurthy, P.; Adaiikkalam, P. pH-potential diagrams at elevated temperatures for the chromium/water systems. *Corros. Sci.* **1982**, *22*, 753–773. [[CrossRef](#)]
84. Fattah-alhosseini, A.; Taheri Shoja, S.; Heydari Zebardast, B.; Mohamadian Samim, P. An Electrochemical Impedance Spectroscopic Study of the Passive State on AISI 304 Stainless Steel. *Int. J. Electrochem.* **2011**, *2011*, 8. [[CrossRef](#)]
85. Castro, B.E.; Vilche, R.J. Investigation of passive layers on iron and iron-chromium alloys by electrochemical impedance spectroscopy. *Electrochim. Acta* **1993**, *38*, 1567–1572. [[CrossRef](#)]
86. Martínez-Villafane, A.; Chacon-Nava, J.G.; Gaona-Tiburcio, C.; Almeraya-Calderon, F.; Dominguez-Patino, G.; Gonzalez-Rodriguez, J.G. Oxidation performance of a Fe–13Cr alloy with additions of rare earth elements. *Mater. Sci. Eng. A* **2003**, *363*, 15–19. [[CrossRef](#)]
87. Cabral Miramontes, J.A.; Barceinas Sánchez, J.D.O.; Almeraya Calderón, F.; Martínez Villafañe, A.; Chacón Nava, J.G. Effect of Boron Additions on Sintering and Densification of a Ferritic Stainless Steel. *J. Mater. Eng. Perform.* **2010**, *19*, 880–884. [[CrossRef](#)]
88. Hryniewicz, T.; Rokosz, K.; Rokicki, R. Electrochemical and XPS studies of AISI 316L stainless steel after electropolishing in a magnetic field. *Corros. Sci.* **2008**, *50*, 2676–2681. [[CrossRef](#)]
89. Hermas, A.A. XPS analysis of the passive film formed on austenitic stainless steel coated with conductive polymer. *Corros. Sci.* **2008**, *50*, 2498–2505. [[CrossRef](#)]
90. Zhidkov, I.S.; Kukhareenko, A.I.; Makarov, A.V.; Savrai, R.A.; Gavrilov, N.V.; Cholakh, S.O.; Kurmaev, E.Z. XPS characterization of surface layers of stainless steel nitrated in electron beam plasma at low temperature. *Surf. Coat. Technol.* **2020**, *386*, 125492. [[CrossRef](#)]
91. Natarajan, R.; Palaniswamy, N.; Natesan, M.; Muralidharan, V.S. XPS analysis of passive film on stainless steel. *Corros. J.* **2009**, *2*, 114–124. [[CrossRef](#)]
92. Jung, R.H.; Tsuchiya, H.; Fujimoto, S. XPS characterization of passive films formed on Type 304 stainless steel in humid atmosphere. *Corros. Sci.* **2012**, *58*, 62–68. [[CrossRef](#)]
93. Mesquita, T.J.; Chauveau, E.; Mantel, M.; Nogueira, R.P. A XPS study of the Mo effect on passivation behaviors for highly controlled stainless steels in neutral and alkaline conditions. *Appl. Surf. Sci.* **2013**, *270*, 90–97. [[CrossRef](#)]
94. Macdonald, D.D. The history of the Point Defect Model for the passive state: A brief review of film growth aspects. *Electrochim. Acta* **2011**, *56*, 1761–1772. [[CrossRef](#)]
95. Jinlong, L.; Tongxiang, L.; Chen, W.; Limin, D. Comparison of corrosion properties of passive films formed on coarse grained and ultrafine grained AISI 2205 duplex stainless steels. *J. Electroanal. Chem.* **2015**, *757*, 263–269. [[CrossRef](#)]
96. Feng, Z.; Cheng, X.; Dong, C.; Xu, L.; Li, X. Passivity of 316L stainless steel in borate buffer solution studied by Mott–Schottky analysis, atomic absorption spectrometry and X-ray photoelectron spectroscopy. *Corros. Sci.* **2010**, *52*, 3646–3653. [[CrossRef](#)]